Fig. 1. Sequence and time course of the EEG/PET/task protocol.

and referenced to linked earlobe electrodes was used to record the glossokinetic potential. Impedance was kept below 5 kΩ. EEG and EMG signals were amplified and filtered by bandpass of 1–50 Hz and 10–50 Hz, respectively, and both were digitized at 250 Hz (Neuroscan, Neuroscan Inc. Herndon, VA). EEG and EMG signals during both conditions were segmented into non-overlapping and artifact-free epochs of 1024 ms which allowed a 1-Hz frequency resolution after Fourier transformation. Epochs with unwanted muscle activity were excluded from the analysis. Power spectra were computed by a fast Fourier transform algorithm implemented on the Neuroscan software. Based on the previous studies (Andres et al., 1999; Mima et al., 2000), the power spectra were grouped into four different frequency bands, 8–12 Hz (alpha), 13–20 Hz (beta1), 21–30 Hz (beta2), and 31–50 Hz (gamma). Since the high and low alpha band rhythms (Klimesch, 1999) behaved quite similarly in our experiment using the simple tasks, we analyzed the whole alpha band as one group. Although the gamma band activity is of special importance for cognition (Rodriguez et al., 1999; Tallon-Baudry and Bertrand, 1999), we did not analyze the gamma band activity because of the environmental electromagnetic noise in the PET scanning room and the possible contamination of EMG. In addition to the 60 Hz noise, the possible contamination of the muscle activity to the occipital electrodes because of the increased neck muscle tone was inevitable due to the tight head fixation for the PET scanning in a few subjects. The local EEG power was calculated by the averaging the EEG powers at 2 electrodes (FC3/C3, FC4/C4, and O1/O2) that were obtained during the PET procedure (60 s). A logarithmic transformation was applied to normalize the power (Halliday et al., 1995).

PET acquisition

$H_2{}^{15}O$ PET scans were obtained in 3D mode using a GE Advance PET tomograph (GE Medical System, Milwaukee, WI) with an axial field of view of 15.3 cm. The task performance began 30 s before bolus infusion of 10 mCi of $H_2{}^{15}O$ (half life 2.1 min) via a catheter in the left cubital vein. Scanning was started when a rising brain radioactivity count was first detected (20–30 s) after injecting the radio-isotope. Scanning continued for 60 s thereafter. Inter-scan interval was 10 min. A transmission scan obtained prior to each session was used to correct for attenuation. Head movement was minimized by using a thermoplastic mask that was molded to each subject's head and attached to the scanner bed. Each subject underwent 10

consecutive PET scans (2 scans for each task). The sequence and time course of the PET/EEG/task protocol are shown in Fig. 1.

Data analysis

The attenuation-corrected emission scans were reconstructed into 35 trans-axial planes, 4.25 mm apart, with an in-plane center resolution of 6.5 mm full width at half-maximum (FWHM) in each direction. Scans from each subject were realigned to correct the head motion during the study then normalized to a standard bicommissural stereotactic space (using Montreal Neurological Institute template) and smoothed with an isotropic Gaussian filter of 12 mm using SPM2 (Wellcome Department of Cognitive Neurology, London, UK) implemented in Matlab (Friston et al., 1990, 1991, 1995). After correction for variations in global blood flow (normalized to 50 ml/100 g/min) using analysis of covariance (ANCOVA), the multi-subject, covariate only design matrix was specified and the subjects with logarithmic EEG power during each task as a covariate were estimated according to the general linear model at each and every voxel, assuming a linear relationship between rCBF and the covariate. Both positive and negative correlations at each voxel were estimated for the occipital, left sensorimotor, and right sensorimotor EEG power. Therefore, the EEG bands of alpha, beta1, and beta2 were adopted in the right and left sensorimotor and occipital regions and a total of 9 covariates were included in separate design matrices. The occipital EEG power was also considered in both sensorimotor EEG power analyses as a nuisance factor because the occipital alpha and beta EEG could have an influence on the sensorimotor EEG.

The resulting whole brain statistical parametric maps of t-statistic (SPM(t)) had a final spatial resolution of 12.6 × 13.7 × 15.0 mm FWHM. The SPM(t) map was transformed into units of normal distribution (SPM(z)), where the significance of each region was estimated with a threshold of uncorrected $p < 0.001$. This uncorrected threshold is commonly used in SPM (Benoit et al., 2002; Salmon et al., 2000; Staff et al., 2000). Because of a large number of statistical comparisons in this voxel-by-voxel analysis, the Bonferroni correction was done to eliminate the probability of a type-I error. Because the Bonferroni correction is the most conservative correction for multiple comparisons and might result in a type-II error, statistical parametric maps that survived a threshold of $p < 0.001$ uncorrected for multiple comparisons were also shown. A higher threshold presented by a corrected $p < 0.05$ at cluster levels was also applied in order to

exclude the clusters that have any probability of being randomly produced (Bench et al., 1992; Salmon et al., 2000; Staff et al., 2000). The SPM coordinates for standard brain from Montreal Neurological Institute were converted to Talairach coordinates (Talairach and Tournoux, 1988) by a non-linear transform method (see http://www.mrc-cbu.cam.ac.uk/Imaging/Common/mnispace. shtml).

Results

The mean movement frequencies during the tasks (task 3, 4 and 5) were 1.3±0.3 Hz in RH, 1.2±0.2 Hz in LH and 1.3± 0.3 Hz in RF (no significant differences). The mean EEG alpha frequencies were 9.8±0.9 Hz in the occipital area, 10.8± 2.1 Hz in the left sensorimotor area and 11.0±1.5 Hz in the right sensorimotor area (no significant differences). The logarithmic regional EEG band power is shown in Fig. 2.

Brain regions correlated with the occipital EEG power

A significant negative correlation between the occipital alpha power and rCBF was found in the bilateral occipital cortices including the primary and association visual cortex (Fig. 3A, Table 1A). Similarly a negative correlation between the occipital beta1 power and rCBF was found in the bilateral occipital cortices (Fig. 3B, Table 1A). A significant negative correlation

between the occipital beta2 power and rCBF was found in the posterior part of the right middle temporal gyrus (Fig. 3C, Table 1A). A significant positive correlation between the occipital alpha power and rCBF was found in both lateral and medial prefrontal cortices and basal forebrain mainly on the left. The left superior temporal gyrus also showed a positive correlation (Fig. 3A, Table 1B). A significant positive correlation between the occipital beta1 power and rCBF was also found in both lateral and medial prefrontal cortices and the left superior temporal gyrus (Fig. 3B, Table 1B). No significant positive correlation was found between the occipital beta2 power and rCBF was found (Fig. 3C, Table 1B).

Brain regions correlated with the left sensorimotor EEG power

A significant negative correlation between the left sensorimotor alpha power and rCBF was found in the left pre- and postcentral gyrus and the left inferior parietal lobule (Fig. 4A, Table 2A). A significant negative correlation between the left sensorimotor beta1 power and rCBF was also found in the left pre- and postcentral gyrus (Fig. 4B, Table 2A). A significant negative correlation between the left sensorimotor beta2 power and rCBF was found in the left postcentral gyrus and inferior parietal lobule (Fig. 4C, Table 2A). No significant positive correlation between the left sensorimotor EEG power and rCBF was found (Figs. 4A–C, Table 2B).
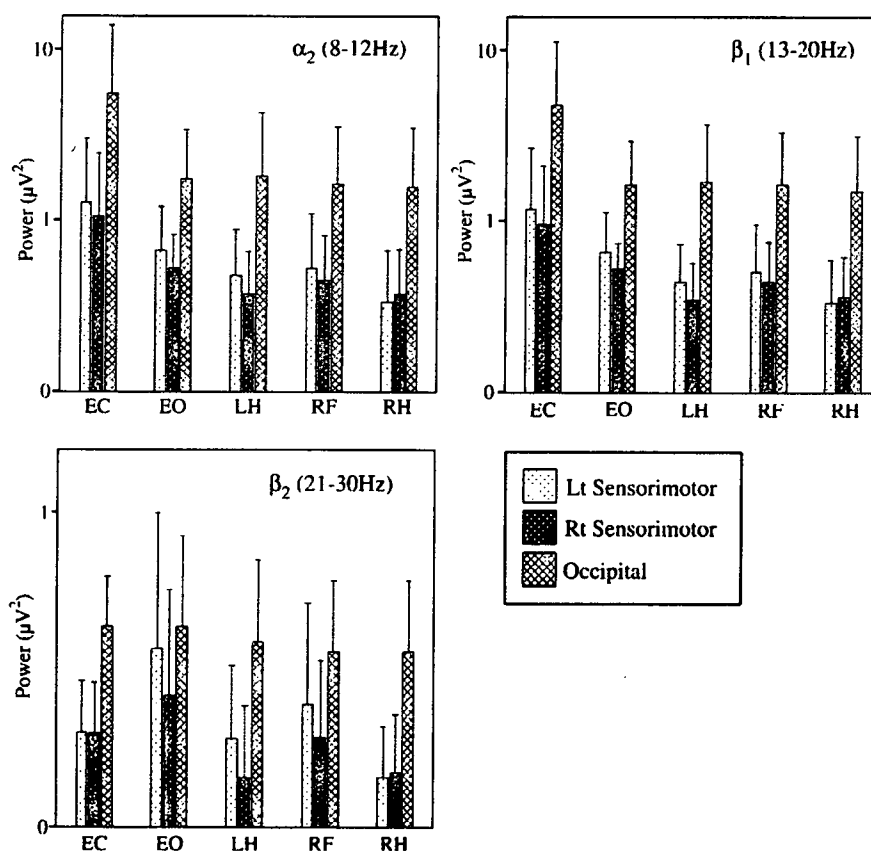

Fig. 2. Plot (mean values + standard deviation) of absolute regional EEG band power. EC, eyes closed; EO, eyes open; LH, left thumb movement; RH, right thumb movement; RF, right foot movement.
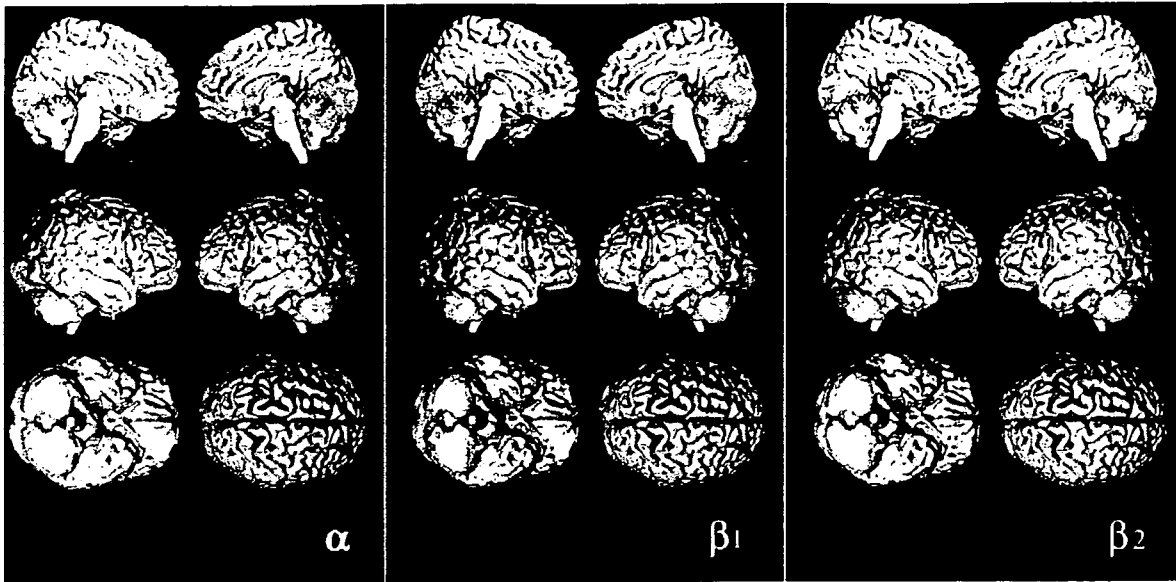
Fig. 3. Statistical parametric maps of positive (yellow-red) and negative (aqua-blue) correlation between rCBF and occipital EEG alpha, beta1 and beta2 power during each task, superimposed on surface-rendered MRI. Areas that survived a statistical threshold of $p<0.001$ uncorrected for multiple comparisons are shown. A significant negative correlation between the occipital alpha and beta1 power and rCBF was found in the bilateral occipital cortices. A significant positive correlation between the occipital alpha and beta1 power and rCBF was also found in both lateral and medial prefrontal cortices.

Brain regions correlated with the right sensorimotor EEG power

A significant negative correlation between the right sensorimotor alpha power and rCBF was found in the right postcentral gyrus and inferior parietal lobule (Fig. 5A, Table 3A). A significant negative correlation between each of the right sensorimotor beta1 and beta2 power and rCBF was also found in the right postcentral gyrus and inferior parietal lobule (Figs. 5B–C, Table 3A). A significant positive correlation between the right sensorimotor alpha power and rCBF was found in the left middle frontal gyrus (Fig. 5A, Table 3B).

Table 1
Brain regions (A) negatively and (B) positively correlated with the occipital EEG power

EEG band	Region	BA	Coordinate Talairach space			Cluster-level corrected P	kE	z
			x	y	z			
(A) Negative correlation								
Alpha	Rt lingual gyrus (GL)	19	20	−78	−11	0.000	9807	5.49
	Rt cuneus	18	10	−101	9			5.35
	Lt lingual gyrus (GL)	18	−8	−80	−13			5.29
	Lt fusiform gyrus (GF)	19	−22	−53	−11	0.003	456	5.10
Beta1	Rt lingual gyrus (GL)	19	20	−11	−11	0.000	9278	5.33
	Lt lingual gyrus (GL)	18	−8	−80	−13			5.16
	Rt cuneus	18	10	−101	9			5.12
	Lt fusiform gyrus (GF)	19	−24	−53	−12	0.006	398	4.99
Beta2	Rt middle temporal gyrus (GTm)	37	50	−62	3	0.011	358	4.10
(B) Positive correlation								
Alpha	Lt anterior cingulate	32	−8	44	−9	0.000	6018	5.27
	Lt superior temporal gyrus (GTs)	38	−49	22	−18	0.000	882	4.60
	Lt precentral gyrus (GPrC)	9	−38	13	34	0.025	289	4.34
	Lt middle frontal gyrus (GFm)	8	−46	10	42			3.62
	Rt middle frontal gyrus (GFm)	8	30	31	43	0.006	399	4.23
Beta1	Rt anterior cingulate	32	12	29	−6	0.000	5714	5.30
	Lt anterior cingulate	32	−8	44	−7			5.16
	Lt superior temporal gyrus (GTs)	38	−49	22	−18	0.000	703	4.39
	Rt middle frontal gyrus (GFm)	8	32	31	41	0.002	507	4.20
	Rt superior frontal gyrus (GFs)	8	40	20	51			3.65
Beta2	No suprathreshold clusters							

Clusters that survived a statistical threshold of $p<0.05$ corrected for multiple comparisons are shown.
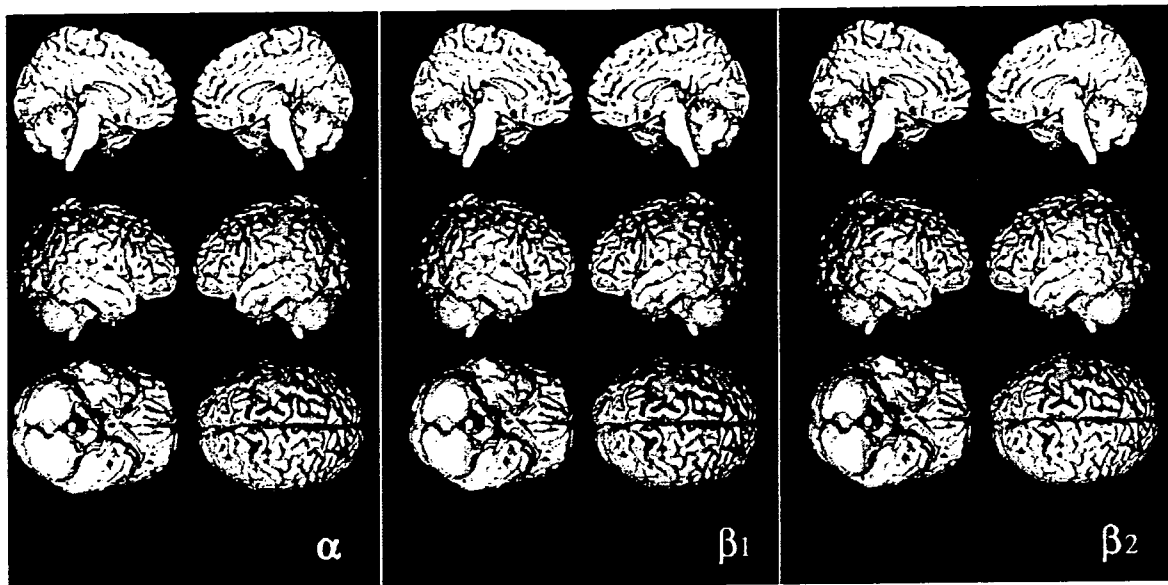
Fig. 4. Statistical parametric maps of positive (yellow-red) and negative (aqua-blue) correlation between rCBF and left sensorimotor EEG alpha, beta1 and beta2 power during each task, superimposed on surface-rendered MRI. Areas that survived a statistical threshold of $p < 0.001$ uncorrected for multiple comparisons are shown. A significant negative correlation between the left sensorimotor alpha and beta1 power and rCBF was found in the left pre- and postcentral gyrus. A significant negative correlation between the left sensorimotor beta2 power and rCBF was found in the left postcentral gyrus.

A significant positive correlation between the right sensorimotor beta1 power and rCBF was found in the left lateral prefrontal cortex and the left superior occipital gyrus (Fig. 5B, Table 3B). No significant positive correlation was found between the right sensorimotor beta2 power and rCBF was found (Fig. 5C, Table 3B).

Discussion

This is the first report of quantitative evaluation of the correlation between rCBF changes and regional EEG powers. Significant negative correlations between the occipital EEG power within the

alpha and lower beta bands and the occipital rCBF were observed. There were also significant negative correlations between the left and right sensorimotor EEG power within the alpha and beta ranges and the ipsilateral sensorimotor rCBF, respectively. These findings suggest that decrease in the regional EEG rhythm at around 10–20 Hz might represent the neuronal activation of the cortex underlying the electrodes, at least for the visual and sensorimotor areas. Since the animal experiments suggested that low amplitude desynchronized EEG is associated with the increased excitability in thalamocortical system (Steriade and Llinas, 1988), it is possible that the decrease of human scalp-recorded EEG power reflects cortical activation (Pfurtscheller, 1992).

Table 2
Brain regions (A) negatively and (B) positively correlated with the left sensorimotor EEG power

EEG band	Region	BA	Coordinate Talairach space			Cluster-level corrected P	kE	z
			x	y	z			
(A) Negative correlation								
Alpha	Lt precentral gyrus (GPrC)	4	−32	−25	51	0.000	1550	5.19
	Lt postcentral gyrus (GPoC)	3	−38	−19	47			5.06
	Lt inferior parietal lobule (LPi)	40	−40	−31	35			3.70
Beta1	Lt precentral gyrus (GPrC)	4	−30	−25	49	0.000	1396	4.96
	Lt postcentral gyrus (GPoC)	3	−38	−19	47			4.79
Beta2	Lt postcentral gyrus (GPoC)	2	−51	−21	45	0.000	964	4.58
	Lt inferior parietal lobule (LPi)	40	−42	−27	42			3.95
	Lt postcentral gyrus (GPoC)	40	−61	−22	18			3.52
(B) Positive correlation								
Alpha	No suprathreshold clusters							
Beta1	No suprathreshold clusters							
Beta2	No suprathreshold clusters							

Clusters that survived a statistical threshold of $p < 0.05$ corrected for multiple comparisons are shown.
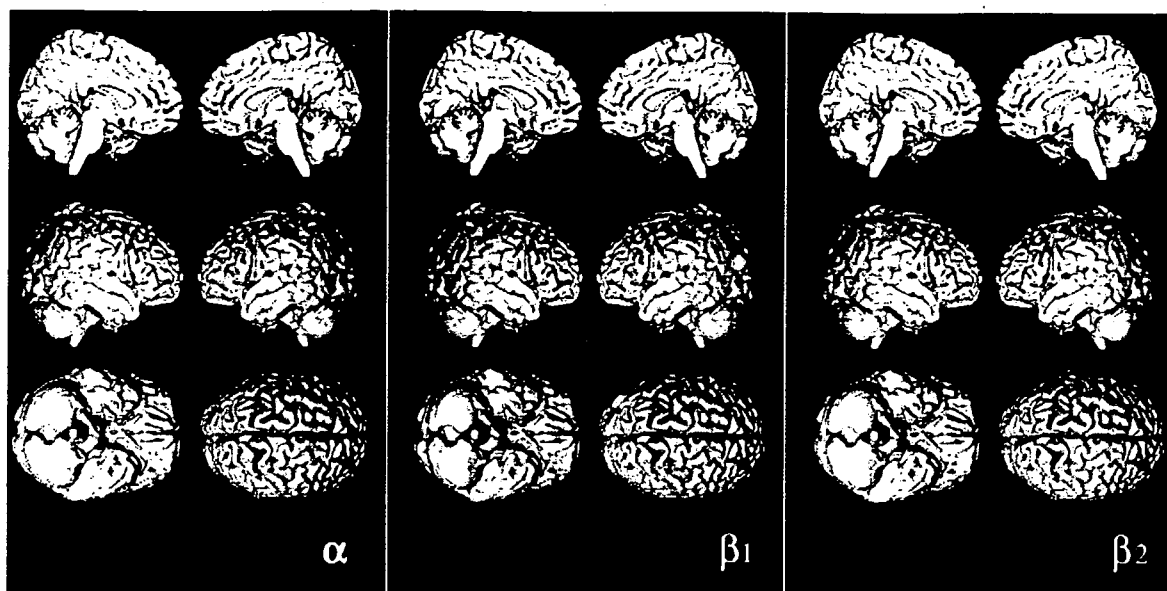
Fig. 5. Statistical parametric maps of positive (yellow-red) and negative (aqua-blue) correlation between rCBF and right sensorimotor EEG alpha, beta1 and beta2 power during each task, superimposed on surface-rendered MRI. Areas that survived a statistical threshold of $p<0.001$ uncorrected for multiple comparisons are shown. A significant negative correlation between the right sensorimotor alpha, beta1 and beta2 power and rCBF was found in the right postcentral gyrus. A significant positive correlation between the right sensorimotor alpha and beta1 power and rCBF was found in the left middle frontal gyrus.

The occipital EEG power showed a positive correlation especially with the rCBF of the prefrontal cortex and the right sensorimotor EEG power showed a positive correlation with the rCBF of the left prefrontal cortex. These results suggest that the neural network including the prefrontal cortex especially on the left could play an important role to generate the EEG rhythm in both occipital and sensorimotor cortices.

Negative correlations of rCBF with the sensorimotor mu rhythm

By investigating the linear relationship between the sensorimotor alpha power and rCBF, we showed that the left and right mu

rhythms have a significant negative correlation with the ipsilateral sensorimotor cortical activation. Because differences in source localization, frequency, power, and functional responsiveness suggest independent sources for mu and occipital alpha rhythms (Pineda, 2005), we performed the rCBF correlation analysis using SPM by setting the occipital alpha power as a statistical nuisance value to evaluate the purely sensorimotor mu rhythm, although the general linear model might not properly eliminate the "nuisance" effect. In addition, we evaluated multiple motor tasks in the present study to minimize a task-specific effect on rCBF change.

Although overlapping each other in the frequency range, the sensorimotor mu and occipital alpha band rhythms rather reflect

Table 3

Brain regions (A) negatively and (B) positively correlated with the right sensorimotor EEG power

EEG band	Region	BA	Coordinate Talairach space			Cluster-level corrected P	kE	z
			x	y	z			
(A) Negative correlation								
Alpha	Rt inferior parietal lobule (LPi)	40	40	−33	44	0.034	266	4.23
	Rt postcentral gyrus (GPoC)	3	36	−23	47			3.37
Beta1	Rt inferior parietal lobule (LPi)	40	42	−35	44	0.001	529	4.44
	Rt postcentral gyrus (GPoC)	3	36	−23	47			3.72
Beta2	Rt inferior parietal lobule (LPi)	40	46	−34	57	0.001	570	4.33
	Rt postcentral gyrus (GPoC)	40	44	−27	47			3.85
	Rt postcentral gyrus (GPoC)	3	53	−23	38			3.56
(B) Positive correlation								
Alpha	Lt middle frontal gyrus (GFm)	10	−32	49	−1	0.037	261	4.48
Beta1	Lt middle frontal gyrus (GFm)	10	−30	47	−2	0.048	242	4.28
	Lt inferior frontal gyrus (GFi)	10	−36	45	5			3.76
	Lt middle frontal gyrus (GFm)	11	−24	40	−9			3.33
	Lt superior occipital gyrus (GOs)	19	−32	−76	24	0.021	300	4.27
Beta2	No suprathreshold clusters							

Clusters that survived a statistical threshold of $p<0.05$ corrected for multiple comparisons are shown.

two distinct physiological phenomena, which was also supported by the present results (Vanni et al., 1999). It has been reported that self-paced hand movement can induce a contralateral localized mu rhythm ERD and an occipital localized alpha band rhythm ERS at the same time (Pfurtscheller and Lopes da Silva, 1999). In direct recordings from cat visual and somatosensory cortices while both alpha and mu rhythms occurred under similar behavioral conditions, their bursts were independent and had low coherence (Rougeul-Buser and Buser, 1997).

In human scalp EEG, the main peak frequency of the mu rhythm is within the alpha band, which mainly covers a frequency range between 7 and 14 Hz with a mean frequency around 10 Hz or even slightly below (Pfurtscheller et al., 2000). However, its distribution is over the bilateral hand SM1, and its power is particularly sensitive to the motor tasks. The blocking of mu rhythm caused by movements of the body part is specific to somatic representation areas of the cortex (Arroyo et al., 1993). The time course of the mu rhythm amplitude shows a specific biphasic pattern, which is known as ERS/ERD (Pfurtscheller, 1977; Pfurtscheller and Lopes da Silva, 1999). Consequently, the 10-Hz mu rhythm increase might reflect a resting state or even inhibition in the sensorimotor system (Pfurtscheller, 1992; Salmelin and Hari, 1994). Our findings are in accord with the 'idling' rhythm hypothesis of the mu rhythm (Kuhlman, 1978). Moreover, the power suppression of the mu rhythm produced by a motor task (Crone et al., 1998; Gerloff et al., 1998; Pfurtscheller and Berghold, 1989; Toma et al., 2002; Toro et al., 1994) may reflect cortical activation at SM1 in a parametric way.

Although the limited spatial resolution of the rCBF measurement using PET cannot allow us to precisely differentiate S1 and M1, the parietal cortex including the postcentral gyrus and inferior parietal lobule showed a greater negative correlation than the frontal cortex including the precentral gyrus in this study. The previous PET study using a simple repetitive finger movement task also showed activation of both S1 and M1 (Mima et al., 1999). The activation of S1 may be due to the somatosensory afferent feedback from the periphery or the motor efferent copy conveyed from M1. It is also possible that the activity of S1 is related to preparation for motor action because some studies showed attenuation of the postcentral mu rhythm prior to voluntary movements (Nagamine et al., 1996; Ohara et al., 2000; Salmelin et al., 1995). Based on the recent results showing a specific motor deficit in movement initiation after an inferior parietal lobule lesion (Mattingley et al., 1998), the inferior parietal lobule has been suggested as a candidate area for higher-order motor function. Since coherent cell assemblies over at least several square centimeters are necessary (Cooper et al., 1965; Lopes da Silva, 1991) for the generation of the scalp-recorded EEG rhythmicity, both M1 and the parietal cortex are likely to be associated with the 'idling' of the mu rhythm.

Negative correlations of rCBF with the sensorimotor beta band rhythm

In this study, the activated areas that were negatively correlated with the sensorimotor alpha, beta1 and beta2 power showed similar cortical distributions. It has been well accepted that the beta band rhythm at SM1 might play an important role in motor control. Cortico-muscular coherence studies suggested that the central beta band rhythm may convey the motor command from M1 to the motor units (Conway et al., 1995; Mima et al., 2000; Salenius et

al., 1996). It has also been reported that the somatosensory beta band rhythms around 18 Hz in monkeys distribute over the SI hand area and the posterior parietal cortex and are blocked by the smallest body movement (Rougeul et al., 1979). Beta desynchronization during voluntary hand movement occurred in parallel with the mu ERD in the alpha band (Pfurtscheller, 1981).

Electrocorticogram and magnetoencephalography studies suggested that the 10 Hz rhythm could appear to arise from the somatosensory cortex, whereas the 20 Hz rhythm could arise predominantly from the precentral gyrus (Hari and Salmelin, 1997; Pfurtscheller, 1992; Salmelin et al., 1995; Salmelin and Hari, 1994). However, this topographic distribution is still controversial because electrocorticogram studies showed no consistent difference in distribution between the 10 Hz rhythm and the 20 Hz rhythm (Crone et al., 1998; Ohara et al., 2000). The rCBF changes in our study did not reveal this anterior–posterior tendency. However, this might be due to the limited spatial resolution of the PET methodology.

Negative correlations of rCBF with the occipital rhythm

The thalamocortical and corticocortical systems are supposed to interact in the generation of cortical alpha band rhythms (Steriade et al., 1990). In this study, the occipital alpha EEG had a significant negative correlation with the bilateral occipital rCBF, which extended broadly from the primary to association cortex. The result is in accordance with the previous reports (Leuchter et al., 1999; Sadato et al., 1998). Extensive involvement of the primary and association visual cortex is consistent with the finding that the alpha band rhythm can be suppressed not only by opening of the eyes but also by visual imagery, which suggests that the suppression of alpha band rhythm can be associated with higher visual processing (Hari and Salmelin, 1997).

Although previous studies revealed that the rCBF change (Larson et al., 1998; Sadato et al., 1998) or the glucose metabolic change (Schreckenberger et al., 2004) in the thalamus correlates with the global alpha power, our result showed no significant correlation between the regional occipital alpha EEG and the activation of thalamus. Therefore, it is possible that the generator mechanism of the whole brain alpha band rhythm and regional (occipital) alpha band rhythm might be different and that the thalamus is related to the production of the former but not so much for the latter. Electrophysiological evidence from isolated cerebral cortex determined that cortical circuits were capable of generating alpha band rhythms quite independently of thalamic influences (Kristiansen and Courtois, 1949). In addition, it has been reported that the corticocortical alpha coherence values were higher than any thalamocortical coherence (da Silva et al., 1973; Lopes da Silva et al., 1980) and relatively independent of thalamic influences (Lopes da Silva et al., 1980).

In this study, a similar correlation with rCBF was observed for the occipital alpha and beta1 power. When a subject concentrates on a particular modality, the EEG activity in the alpha and/or lower beta band specifically decreases in the corresponding brain region (Neuper and Pfurtscheller, 2001). Therefore, our result suggests that the same neurophysiological mechanism as the occipital alpha band rhythm could be associated with the occipital beta1 band rhythm generation. However, the similar correlation might be caused by a harmonic of the alpha activity because alpha activity is often not sinusoidal and it is very difficult to differentiate such a harmonic from beta band rhythms.

Positive correlations of rCBF with the sensorimotor and occipital rhythm

A significant positive correlation was found between the right sensorimotor alpha power and the rCBF of the left middle prefrontal gyrus, which extended to the dorsolateral prefrontal cortex (BA 9/46) (Ramnani and Owen, 2004). The sensorimotor mu rhythm is associated with motor behavior (Pfurtscheller et al., 1996). Although no direct connections have been reported between the dorsolateral prefrontal cortex and SM1, the dorsolateral prefrontal cortex sends the strongest projections to the premotor system in the macaque monkey brain (Lu et al., 1994). The premotor area could influence motor control (Tokuno and Nambu, 2000) via its dense corticocortical projections to M1 (Dum and Strick, 2002; Shimazu et al., 2004). Our result suggests that the corticocortical network between the prefrontal cortex and the SM1 via the premotor cortex might be associated with the generation of the sensorimotor mu rhythm, especially on the right. On the other hand, the left sensorimotor EEG power did not show any significant positive correlations. The EEG study using an independent component analysis suggested independent mu sources in the two hemispheres (Makeig et al., 2002). Therefore, the asymmetric results in our study might explain the independent generation of the sensorimotor mu rhythm in the two hemispheres. However, further researches would be necessary to elucidate the exact role of left middle frontal gyrus for the generation of mu rhythm.

A significant positive correlation between the right sensorimotor beta1 power and rCBF was found in the left lateral prefrontal cortex which is similar to the right sensorimotor mu power. Our result suggests that the corticocortical network including the prefrontal cortex and SM1 could be associated with the generation of the sensorimotor beta1 band rhythm as well as the mu rhythm in the alpha band. In a previous study (Nakamura et al., 1999), the rCBF in the left lateral prefrontal cortex was demonstrated to be positively correlated with the global beta power. Beta activity has recently been ascribed to the general role of an 'attention-carrier' (Wrobel, 2000) and associated with behavioral arousal and attentional processes (Nofzinger et al., 2000). States of attention and motor preparation were suggested to be particularly associated with increased levels of beta activity in the cat (Bouyer et al., 1981) and the monkey motor cortex (Rougeul et al., 1979) in local field potential studies. These reports suggest that focused attention for the motor preparation might be associated with the sensorimotor beta1 band rhythm and the prefrontal cortex (Steriade, 1993).

A significant positive correlation between the occipital alpha power and rCBF was found in both lateral and medial prefrontal cortices and basal forebrain mainly on the left, which is consistent with the previous study (Sadato et al., 1998) that showed a positive correlation between the alpha power and the rCBF in the limbic system including basal prefrontal cortex. A similar positive correlation was also found between the occipital beta1 power and rCBF. The orbitofrontal cortices are associated with social–affective and motivational aspects of frontal lobe function (Rolls, 2004). Anatomically, the orbitofrontal cortices have widespread connections with a distributed ascending activating system including the pontine reticular formation, basal forebrain, amygdala, hippocampus, temporal pole, insula, cingulate cortex and parahippocampal gyrus (Morecraft et al., 1992), placing them in a position to integrate limbic–paralimbic afferents with those coming from higher order association cortex and subsequently influence motivational, emotional and arousal systems in the brain (Nofzinger et al., 2000). The

positive correlation between the occipital alpha and beta1 power and neuronal activities in the limbic system including anterior cingulate cortex and orbitofrontal cortex may provide a neuroanatomical basis for studies of the relationship between emotional state and occipital alpha and beta1 band rhythm. The global alpha band rhythms have also been explored as a possible indicator of emotional states (Drennen and O'Reilly, 1986) and increased attention has been focused on the association of local alpha oscillations, including the occipital alpha oscillations, with cognitive operations (Klimesch, 1996, 1997). An interaction between anterior and posterior cortical circuits in the generation of human alpha rhythms has been supported by EEG coherence studies (Cantero et al., 1999, 2000; Srinivasan, 1999; Thatcher et al., 1986). This functional relationship could be anatomically supported by the superior longitudinal fasciculus traveling parallel to the midline (Cantero et al., 2002).

These findings suggest that the neural network for generating the EEG rhythm in both occipital and sensorimotor cortices might be similar and nonspecific. Studies using the frontal midline (mental) theta activities suggest that the prefrontal cortex including the anterior cingulate cortex might work as a generator of the state of internalized attention, which means manipulation of one's attentional focus during meditation (Aftanas and Golocheikine, 2001; Ishii et al., 1999; Sasaki et al., 1996). Thus, it is likely that the apparent positive correlation between the prefrontal activation and the increased idling rhythm at the sensorimotor or visual cortex can be due to the state of internalized attention facilitated by the rest condition with eyes closed.

EEG and PET methodology

Although the $H_2^{15}O$ tracer has much shorter time frame than the 18-fluoro-deoxyglucose tracer (20–30 min) and the results of $H_2^{15}O$ PET examinations directly depend on the acute cerebral state of activation during tracer injection (Schreckenberger et al., 2004), it is also true that the simultaneous PET and EEG recordings reflect EEG signals and cerebral blood flow changes which were temporally averaged over the span of 60 s. This diminished time resolution may be one of the limitations of the inter-modality correlation. However, it is likely that the EEG power should be stable during the PET scan time in the present study because we applied the simple repetitive movement tasks, in which the estimation of the task-related power change of the EEG was found to be useful (Andres et al., 1999; Gerloff et al., 1998; Toma et al., 2002).

Various types of EEG reference techniques may have different advantages and disadvantages for the EEG power estimation (Nunez et al., 1997). In the present study, we used the digitally linked earlobe reference. It is possible that the earlobe reference signal may contain the task-related EEG activity. However, none of our EEG electrodes (C3, C4, FC3, FC4, O1, O2) was located closer than ~6 cm to the reference electrodes, which may minimize the contribution of reference activation. To minimize the effect of common reference signal that is inevitably contaminated in the referenced EEG recording, we used the covariance analysis in which the task-related change of the EEG power and the task-related change of rCBF were compared.

Acknowledgments

References

Aftanas, L.I., Golocheikine, S.A., 2001. Human anterior and frontal midline theta and lower alpha reflect emotionally positive state and internalized attention: high-resolution EEG investigation of meditation. Neurosci. Lett. 310, 57–60.

Andres, F.G., Mima, T., Schulman, A.E., Dichgans, J., Hallett, M., Gerloff, C., 1999. Functional coupling of human cortical sensorimotor areas during bimanual skill acquisition. Brain 122, 855–870.

Arroyo, S., Lesser, R.P., Gordon, B., Uematsu, S., Jackson, D., Webber, R., 1993. Functional significance of the mu rhythm of human cortex: an electrophysiologic study with subdural electrodes. Electroencephalogr. Clin. Neurophysiol. 87, 76–87.

Bench, C.J., Friston, K.J., Brown, R.G., Scott, L.C., Frackowiak, R.S., Dolan, R.J., 1992. The anatomy of melancholia-focal abnormalities of cerebral blood flow in major depression. Psychol. Med. 22, 607–615.

Benoit, M., Koulibaly, P.M., Migneco, O., Darcourt, J., Pringuey, D.J., Robert, P.H., 2002. Brain perfusion in Alzheimer's disease with and without apathy: a SPECT study with statistical parametric mapping analysis. Psychiatry Res. 114, 103–111.

Berger, H., 1929. Uber das Elektrenkephalogramm des Menschen. Arch. Psychiatr. Nervenkrankh. 87, 527–570.

Berger, H., 1930. Uber das Elektrenkephalogramm des Menschen, 2nd report. J. Psychol. Neurol. (Leipzig) 40, 160–179.

Berger, H., 1932. Uber das Elektrenkephalogramm des Menschen, 4th report. Arch. Psychiatr. Nervenkrankh. 97, 6–26.

Bouyer, J.J., Montaron, M.F., Rougeul, A., 1981. Fast fronto-parietal rhythms during combined focused attentive behaviour and immobility in cat: cortical and thalamic localizations. Electroencephalogr. Clin. Neurophysiol. 51, 244–252.

Cantero, J.L., Atienza, M., Salas, R.M., Gomez, C.M., 1999. Alpha EEG coherence in different brain states: an electrophysiological index of the arousal level in human subjects. Neurosci. Lett. 271, 167–170.

Cantero, J.L., Atienza, M., Salas, R.M., 2000. State-modulation of cortico-cortical connections underlying normal EEG alpha variants. Physiol. Behav. 71, 107–115.

Cantero, J.L., Atienza, M., Salas, R.M., 2002. Human alpha oscillations in wakefulness, drowsiness period, and REM sleep: different electro-encephalographic phenomena within the alpha band. Neurophysiol. Clin. 32, 54–71.

Chen, R., Yaseen, Z., Cohen, L.G., Hallett, M., 1998. Time course of corticospinal excitability in reaction time and self-paced movements. Ann. Neurol. 44, 317–325.

Conway, B.A., Halliday, D.M., Farmer, S.F., Shahani, U., Maas, P., Weir, A.I., Rosenberg, J.R., 1995. Synchronization between motor cortex and spinal motoneuronal pool during the performance of a maintained motor task in man. J. Physiol. 489, 917–924.

Cooper, R., Winter, A.L., Crow, H.J., Walter, W.G., 1965. Comparison of subcortical, cortical and scalp activity using chronically indwelling electrodes in man. Electroencephalogr. Clin. Neurophysiol. 18, 217–228.

Crone, N.E., Miglioretti, D.L., Gordon, B., Sieracki, J.M., Wilson, M.T., Uematsu, S., Lesser, R.P., 1998. Functional mapping of human sensorimotor cortex with electrocorticographic spectral analysis. I. Alpha and beta event-related desynchronization. Brain 121, 2271–2299.

da Silva, F.H., van Lierop, T.H., Schrijer, C.F., van Leeuwen, W.S., 1973. Organization of thalamic and cortical alpha rhythms: spectra and coherences. Electroencephalogr. Clin. Neurophysiol. 35, 627–639.

Drennen, W.T., O'Reilly, B.K., 1986. Alpha enhancement: a comparison study of biofeedback, open focus training, and control procedures. Percept. Mot. Skills 62, 467–474.

Dum, R.P., Strick, P.L., 2002. Motor areas in the frontal lobe of the primate. Physiol. Behav. 77, 677–682.

Erecinska, M., Silver, I.A., 1989. ATP and brain function. J. Cereb. Blood Flow Metab. 9, 2–19.

Feng, C.M., Narayana, S., Lancaster, J.L., Jerabek, P.A., Arnow, T.L., Zhu, F., Tan, L.H., Fox, P.T., Gao, J.H., 2004. CBF changes during brain activation: fMRI vs. PET. NeuroImage 22, 443–446.

Friston, K.J., Frith, C.D., Liddle, P.F., Dolan, R.J., Lammertsma, A.A., Frackowiak, R.S., 1990. The relationship between global and local changes in PET scans. J. Cereb. Blood Flow Metab. 10, 458–466.

Friston, K.J., Frith, C.D., Liddle, P.F., Frackowiak, R.S., 1991. Comparing functional (PET) images: the assessment of significant change. J. Cereb. Blood Flow Metab. 11, 690–699.

Friston, K.J., Holmes, A.P., Worsley, K.J., Poline, J.B., Frith, C.D., Frackowiak, R.S., 1995. Statistical parametric maps in functional imaging: a general linear approach. Hum. Brain Mapp. 2, 189–210.

Gerloff, C., Richard, J., Hadley, J., Schulman, A.E., Honda, M., Hallett, M., 1998. Functional coupling and regional activation of human cortical motor areas during simple, internally paced and externally paced finger movements. Brain 121, 1513–1531.

Halliday, D.M., Rosenberg, J.R., Amjad, A.M., Breeze, P., Conway, B.A., Farmer, S.F., 1995. A framework for the analysis of mixed time series/point process data—theory and application to the study of physiological tremor, single motor unit discharges and electromyograms. Prog. Biophys. Mol. Biol. 64, 237–278.

Hari, R., Salmelin, R., 1997. Human cortical oscillations: a neuromagnetic view through the skull. Trends Neurosci. 20, 44–49.

Ingvar, D.H., Sjolund, B., Ardo, A., 1976. Correlation between dominant EEG frequency, cerebral oxygen uptake and blood flow. Electroencephalogr. Clin. Neurophysiol. 41, 268–276.

Ishii, R., Shinosaki, K., Ukai, S., Inouye, T., Ishihara, T., Yoshimine, T., Hirabuki, N., Asada, H., Kihara, T., Robinson, S.E., Takeda, M., 1999. Medial prefrontal cortex generates frontal midline theta rhythm. NeuroReport 10, 675–679.

Klimesch, W., 1996. Memory processes, brain oscillations and EEG synchronization. Int. J. Psychophysiol. 24, 61–100.

Klimesch, W., 1997. EEG-alpha rhythms and memory processes. Int. J. Psychophysiol. 26, 319–340.

Klimesch, W., 1999. EEG alpha and theta oscillations reflect cognitive and memory performance: a review and analysis. Brain Res. Brain Res. Rev. 29, 169–195.

Kristiansen, K., Courtois, G., 1949. Rhythmic electrical activity from isolated cerebral cortex. Electroencephalogr. Clin. Neurophysiol. 3, 265–272.

Kuhlman, W.N., 1978. Functional topography of the human mu rhythm. Electroencephalogr. Clin. Neurophysiol. 44, 83–93.

Larson, C.L., Davidson, R.J., Abercrombie, H.C., Ward, R.T., Schaefer, S.M., Jackson, D.C., Holden, J.E., Perlman, S.B., 1998. Relations between PET-derived measures of thalamic glucose metabolism and EEG alpha power. Psychophysiology 35, 162–169.

Leuchter, A.F., Uijtdehaage, S.H., Cook, I.A., O'Hara, R., Mandelkern, M., 1999. Relationship between brain electrical activity and cortical perfusion in normal subjects. Psychiatry Res. 90, 125–140.

Lopes da Silva, F., 1991. Neural mechanisms underlying brain waves: from neural membranes to networks. Electroencephalogr. Clin. Neurophysiol. 79, 81–93.

Lopes da Silva, F.H., Vos, J.E., Mooibroek, J., Van Rotterdam, A., 1980. Relative contributions of intracortical and thalamo-cortical processes in the generation of alpha rhythms, revealed by partial coherence analysis. Electroencephalogr. Clin. Neurophysiol. 50, 449–456.

Lu, M.T., Preston, J.B., Strick, P.L., 1994. Interconnections between the prefrontal cortex and the premotor areas in the frontal lobe. J. Comp. Neurol. 341, 375–392.

Makeig, S., Westerfield, M., Jung, T.P., Enghoff, S., Townsend, J., Courchesne, E., Sejnowski, T.J., 2002. Dynamic brain sources of visual evoked responses. Science 295, 690–694.

Mattingley, J.B., Husain, M., Rorden, C., Kennard, C., Driver, J., 1998.

Motor role of human inferior parietal lobe revealed in unilateral neglect patients. Nature 392, 179–182.

Mima, T., Hallett, M., 1999. Electroencephalographic analysis of cortico-muscular coherence: reference effect, volume conduction and generator mechanism. Clin. Neurophysiol. 110, 1892–1899.

Mima, T., Sadato, N., Yazawa, S., Hanakawa, T., Fukuyama, H., Yonekura, Y., Shibasaki, H., 1999. Brain structures related to active and passive finger movements in man. Brain 122, 1989–1997.

Mima, T., Matsuoka, T., Hallett, M., 2000. Functional coupling of human right and left cortical motor areas demonstrated with partial coherence analysis. Neurosci. Lett. 287, 93–96.

Morecraft, R.J., Geula, C., Mesulam, M.M., 1992. Cytoarchitecture and neural afferents of orbitofrontal cortex in the brain of the monkey. J. Comp. Neurol. 323, 341–358.

Nagamine, T., Kajola, M., Salmelin, R., Shibasaki, H., Hari, R., 1996. Movement-related slow cortical magnetic fields and changes of spontaneous MEG- and EEG-brain rhythms. Electroencephalogr. Clin. Neurophysiol. 99, 274–286.

Nakamura, S., Sadato, N., Oohashi, T., Nishina, E., Fuwamoto, Y., Yonekura, Y., 1999. Analysis of music–brain interaction with simultaneous measurement of regional cerebral blood flow and electroencephalogram beta rhythm in human subjects. Neurosci. Lett. 275, 222–226.

Neuper, C., Pfurtscheller, G., 2001. Event-related dynamics of cortical rhythms: frequency-specific features and functional correlates. Int. J. Psychophysiol. 43, 41–58.

Niedermeyer, E., Lopes da Silva, F., 1987. Electroencephalography: Basic Principles, Clinical Applications, and Related Fields. Urban and Schwartzenberg.

Nofzinger, E.A., Price, J.C., Meltzer, C.C., Buysse, D.J., Villemagne, V.L., Miewald, J.M., Sembrat, R.C., Steppe, D.A., Kupfer, D.J., 2000. Towards a neurobiology of dysfunctional arousal in depression: the relationship between beta EEG power and regional cerebral glucose metabolism during NREM sleep. Psychiatry Res. 98, 71–91.

Nunez, P.L., Srinivasan, R., Westdorp, A.F., Wijesinghe, R.S., Tucker, D.M., Silberstein, R.B., Cadusch, P.J., 1997. EEG coherency. I: statistics, reference electrode, volume conduction, Laplacians, cortical imaging, and interpretation at multiple scales. Electroencephalogr. Clin. Neurophysiol. 103, 499–515.

Nunez, P.L., Wingeier, B.M., Silberstein, R.B., 2001. Spatial–temporal structures of human alpha rhythms: theory, microcurrent sources, multiscale measurements, and global binding of local networks. Hum. Brain Mapp. 13, 125–164.

Oakes, T.R., Pizzagalli, D.A., Hendrick, A.M., Horras, K.A., Larson, C.L., Abercrombie, H.C., Schaefer, S.M., Koger, J.V., Davidson, R.J., 2004. Functional coupling of simultaneous electrical and metabolic activity in the human brain. Hum. Brain Mapp. 21, 257–270.

Ohara, S., Nagamine, T., Ikeda, A., Kunieda, T., Matsumoto, R., Taki, W., Hashimoto, N., Baba, K., Mihara, T., Salenius, S., Shibasaki, H., 2000. Electrocorticogram–electromyogram coherence during isometric contraction of hand muscle in human. Clin. Neurophysiol. 111, 2014–2024.

Paulson, O.B., Sharbrough, F.W., 1974. Physiologic and pathophysiologic relationship between the electroencephalogram and the regional cerebral blood flow. Acta Neurol. Scand. 50, 194–220.

Pfurtscheller, G., 1977. Graphical display and statistical evaluation of event-related desynchronization (ERD). Electroencephalogr. Clin. Neurophysiol. 43, 757–760.

Pfurtscheller, G., 1981. Central beta rhythm during sensorimotor activities in man. Electroencephalogr. Clin. Neurophysiol. 51, 253–264.

Pfurtscheller, G., 1989. Functional topography during sensorimotor activation studied with event-related desynchronization mapping. J. Clin. Neurophysiol. 6, 75–84.

Pfurtscheller, G., 1992. Event-related synchronization (ERS): an electrophysiological correlate of cortical areas at rest. Electroencephalogr. Clin. Neurophysiol. 83, 62–69.

Pfurtscheller, G., Aranibar, A., 1977. Event-related cortical desynchronization detected by power measurements of scalp EEG. Electroencephalogr. Clin. Neurophysiol. 42, 817–826.

Pfurtscheller, G., Berghold, A., 1989. Patterns of cortical activation during planning of voluntary movement. Electroencephalogr. Clin. Neurophysiol. 72, 250–258.

Pfurtscheller, G., Lopes da Silva, F.H., 1999. Event-related EEG/MEG synchronization and desynchronization: basic principles. Clin. Neurophysiol. 110, 1842–1857.

Pfurtscheller, G., Stancak Jr., A., Neuper, C., 1996. Post-movement beta synchronization. A correlate of an idling motor area? Electroencephalogr. Clin. Neurophysiol. 98, 281–293.

Pfurtscheller, G., Neuper, C., Krausz, G., 2000. Functional dissociation of lower and upper frequency mu rhythms in relation to voluntary limb movement. Clin. Neurophysiol. 111, 1873–1879.

Pineda, J.A., 2005. The functional significance of mu rhythms: translating "seeing" and "hearing" into "doing". Brain Res. Brain Res. Rev. 50, 57–68.

Raichle, M.E., 1987. Circulatory and metabolic correlates of brain function in normal humans. In: Mountcastle, V.B., Plum, F., Geiger, S.R. (Eds.), Handbook of Physiology Section 1: The Nervous System. Volume V. Higher Functions of the Brain. American Physiology Society, Bethesda, pp. 643–674.

Ramnani, N., Owen, A.M., 2004. Anterior prefrontal cortex: insights into function from anatomy and neuroimaging. Nat. Rev., Neurosci. 5, 184–194.

Rodriguez, E., George, N., Lachaux, J.P., Martinerie, J., Renault, B., Varela, F.J., 1999. Perception's shadow: long-distance synchronization of human brain activity. Nature 397, 430–433.

Rolls, E.T., 2004. The functions of the orbitofrontal cortex. Brain Cogn. 55, 11–29.

Rougeul, A., Bouyer, J.J., Dedet, L., Debray, O., 1979. Fast somatoparietal rhythms during combined focal attention and immobility in baboon and squirrel monkey. Electroencephalogr. Clin. Neurophysiol. 46, 310–319.

Rougeul-Buser, A., Buser, P., 1997. Rhythms in the alpha band in cats and their behavioural correlates. Int. J. Psychophysiol. 26, 191–203.

Sadato, N., Nakamura, S., Oohashi, T., Nishina, E., Fuwamoto, Y., Waki, A., Yonekura, Y., 1998. Neural networks for generation and suppression of alpha rhythm: a PET study. NeuroReport 9, 893–897.

Salenius, S., Salmelin, R., Neuper, C., Pfurtscheller, G., Hari, R., 1996. Human cortical 40 Hz rhythm is closely related to EMG rhythmicity. Neurosci. Lett. 213, 75–78.

Salmelin, R., Hari, R., 1994. Spatiotemporal characteristics of sensorimotor neuromagnetic rhythms related to thumb movement. Neuroscience 60, 537–550.

Salmelin, R., Hamalainen, M., Kajola, M., Hari, R., 1995. Functional segregation of movement-related rhythmic activity in the human brain. NeuroImage 2, 237–243.

Salmon, E., Collette, F., Degueldre, C., Lemaire, C., Franck, G., 2000. Voxel-based analysis of confounding effects of age and dementia severity on cerebral metabolism in Alzheimer's disease. Hum. Brain Mapp. 10, 39–48.

Sasaki, K., Nambu, A., Tsujimoto, T., Matsuzaki, R., Kyuhou, S., Gemba, H., 1996. Studies on integrative functions of the human frontal association cortex with MEG. Brain Res. Cogn. Brain Res. 5, 165–174.

Schreckenberger, M., Lange-Asschenfeld, C., Lochmann, M., Mann, K., Siessmeier, T., Buchholz, H.G., Bartenstein, P., Grunder, G., 2004. The thalamus as the generator and modulator of EEG alpha rhythm: a combined PET/EEG study with lorazepam challenge in humans. NeuroImage 22, 637–644.

Shimazu, H., Maier, M.A., Cerri, G., Kirkwood, P.A., Lemon, R.N., 2004. Macaque ventral premotor cortex exerts powerful facilitation of motor cortex outputs to upper limb motoneurons. J. Neurosci. 24, 1200–1211.

Sokoloff, L., 1977. Relation between physiological function and energy metabolism in the central nervous system. J. Neurochem. 29, 13–26.

Sokoloff, L., 1981. Relationships among local functional activity, energy metabolism, and blood flow in the central nervous system. Fed. Proc. 40, 2311–2316.

Srinivasan, R., 1999. Spatial structure of the human alpha rhythm: global correlation in adults and local correlation in children. Clin. Neurophysiol. 110, 1351–1362.

Staff, R.T., Venneri, A., Gemmell, H.G., Shanks, M.F., Pestell, S.J., Murray, A.D., 2000. HMPAO SPECT imaging of Alzheimer's disease patients with similar content-specific autobiographic delusion: comparison using statistical parametric mapping. J. Nucl. Med. 41, 1451–1455.

Steinmetz, H., Furst, G., Meyer, B.U., 1989. Craniocerebral topography within the international 10–20 system. Electroencephalogr. Clin. Neurophysiol. 72, 499–506.

Steriade, M., 1993. Cellular substrates of brain rhythms, In: Niedermeyer, E., Lopes da Silva, F.H. (Eds.), Electroencephalography: Basic Principles, Clinical Applications and Related Fields, 3rd ed. Williams and Wilkins, Baltimore, pp. 27–62.

Steriade, M., Llinas, R.R., 1988. The functional states of the thalamus and the associated neuronal interplay. Physiol. Rev. 68, 649–742.

Steriade, M., Gloor, P., Llinas, R.R., Lopes de Silva, F.H., Mesulam, M.M., 1990. Report of IFCN Committee on Basic Mechanisms. Basic mechanisms of cerebral rhythmic activities. Electroencephalogr. Clin. Neurophysiol. 76, 481–508.

Talairach, J., Tournoux, P., 1988. Co-planar Stereotaxic Atlas of the Human Brain. Thieme, Stuttgart.

Tallon-Baudry, C., Bertrand, O., 1999. Oscillatory gamma activity in humans and its role in object representation. Trends Cogn. Sci. 3, 151–162.

Thatcher, R.W., Krause, P.J., Hrybyk, M., 1986. Cortico-cortical associations and EEG coherence: a two-compartmental model. Electroencephalogr. Clin. Neurophysiol. 64, 123–143.

Tokuno, H., Nambu, A., 2000. Organization of nonprimary motor cortical inputs on pyramidal and nonpyramidal tract neurons of primary motor cortex: an electrophysiological study in the macaque monkey. Cereb. Cortex 10, 58–68.

Toma, K., Mima, T., Matsuoka, T., Gerloff, C., Ohnishi, T., Koshy, B., Andres, F., Hallett, M., 2002. Movement rate effect on activation and functional coupling of motor cortical areas. J. Neurophysiol. 88, 3377–3385.

Toro, C., Deuschl, G., Thatcher, R., Sato, S., Kufta, C., Hallett, M., 1994. Event-related desynchronization and movement-related cortical potentials on the ECoG and EEG. Electroencephalogr. Clin. Neurophysiol. 93, 380–389.

Vanni, S., Portin, K., Virsu, V., Hari, R., 1999. Mu rhythm modulation during changes of visual percepts. Neuroscience 91, 21–31.

Vijn, P.C., van Dijk, B.W., Spekreijse, H., 1991. Visual stimulation reduces EEG activity in man. Brain Res. 550, 49–53.

Wrobel, A., 2000. Beta activity: a carrier for visual attention. Acta Neurobiol. Exp. (Wars.) 60, 247–260.

ORIGINAL PAPER

Yukihisa Suzuki
Shoichi Mizoguchi
Motohiro Kiyosawa
Manabu Mochizuki
Kiichi Ishiwata
Masato Wakakura
Kenji Ishii

Glucose hypermetabolism in the thalamus of patients with essential blepharospasm

Y. Suzuki, MD, PhD
S. Mizoguchi, MD, PhD
M. Kiyosawa, MD, PhD
M. Mochizuki, MD, PhD
Dept. of Ophthalmology and Visual Science
Tokyo Medical and Dental University
Tokyo, Japan

K. Ishiwata, PhD · K. Ishii, MD (✉)
Y. Suzuki, MD, PhD
S. Mizoguchi, MD, PhD
Positron Medical Center
Tokyo Metropolitan Institute
of Gerontology
35-2 Sakaecho
Itabashi, Tokyo, Japan
Tel.: +81-3/3964-3241, ext. 3503
Fax: +81-3/3964-2188
E-Mail: ishii@pet.tmig.or.jp

M. Wakakura, MD, PhD
Inouye Eye Hospital
Tokyo, Japan

■ **Abstract** Essential blepharospasm (EB) is classified as a form of focal dystonia characterized by involuntary spasms of the musculature of the upper face. The basic neurological process causing EB is not known. The purpose of this study was to investigate cerebral glucose metabolism in patients with EB whose symptoms were suppressed by an injection of botulinum-A toxin. Earlier studies were confounded by sensory feedback activities derived from dystonic symptom itself. Cerebral glucose metabolism was examined by positron emission tomography (PET) with ^{18}F-fluorodeoxyglucose (FDG) in 25 patients (8 men and 17 women; age 52.6 ± 10.1 years) with EB. The patients were awake but with the spasms suppressed by an injection of botulinum-A toxin. Thirty-eight normal volunteers (14 men and 24 women; age 58.2 ± 7.3 years) were examined as controls. The difference between the two groups was examined by statistical parametric mapping (SPM99). A significant increase in the glucose metabolism was detected in the thalamus and pons in the EB patients. Hyperactivity in the thalamus may be a key pathophysiological change common to EB and other types of focal dystonia. The activity of the striatum and cerebellum are likely to be sensory dependent.

■ **Key words** essential blepharospasm · focal dystonia · glucose metabolism · positron emission tomography · thalamus

Introduction

Essential blepharospasm (EB) is a form of focal dystonia characterized by involuntary spasms of the musculature of the upper face. Earlier studies have reported a glucose hypermetabolism in the thalamus and basal ganglia in patients with dystonia, and it has been widely held that dysfunction of cortical-striato-thalamo-cortical motor circuits may have a major role in the pathophysiology of dystonia [1]. It has also been reported that dystonia is caused by thalamic infarctions [2], and patients with EB have been reported to be associated with increased glucose metabolism in the thalamus [3] and cerebellum [4] by positron emission tomography (PET) studies using ^{18}F-fluorodeoxyglucose (FDG).

There have been several studies on other forms of focal dystonia using PET. In patients with spasmodic torticollis, Galardi et al. reported hypermetabolism in the thalamus, basal ganglia, anterior cingulate gyrus,

and cerebellum [5], and Eidelberg et al. found a relative increase of metabolic activity in the lentiform nucleus and premotor cortices of patients with idiopathic torsion dystonia [6]. In EB and other dystonias, the majority of the studies have demonstrated a hypermetabolism of the thalamus and basal ganglia. A common limitation of earlier neuroimaging studies of dystonia lies in that they observed integral brain activities reflecting both the cause and the consequence of abnormal involuntary movements.

In order to separate the effects of cause and consequence on EB, Hutchinson et al. measured the glucose metabolism of EB patients during wakefulness and during induced sleep because the involuntary movements disappear during sleep. They found a hypermetabolism in the cerebellum and pons only during wakefulness [4]. However they could not find the primary cause of EB during sleep.

We hypothesized that the hyperactivity in the thalamus and basal ganglia is not a secondary phenomenon accompanies the abnormal movement, but is a primary pathophysiological condition that cause the symptoms. To test this hypothesis and to determine the responsible cerebral regions, PET measurements were made to evaluate regional cerebral glucose metabolism while the patients were awake, but the involuntary eyelid movements were suppressed by a botulinum toxin-A injection.

Materials and methods

Twenty-five patients (8 men and 17 women; age 52.6 ± 10.1 years), who visited the Ophthalmology Outpatient Clinic of Tokyo Medical and Dental University Hospital and were diagnosed with bilateral EB, were studied. The mean duration of their illness was 2.9 ± 3.3 years. None had an organic brain disorder or other neuro-psychiatric disease as evaluated by neurologists from conventional diagnostic magnetic resonance images (MRIs). No one had a family history of dystonic disorders. Patients who had not taken any neuro-psychiatric drugs such as neuroleptic drugs, antidepressant drugs, anti-Parkisonian drugs, and anti-epileptic drugs were selected by careful history taking to exclude drug-related cases because drug related cases might confound [7]. Thirty-eight normal volunteers (14 men and 24 women; age 58.2 ± 7.3 years) were recruited as the normal control group. Normal subjects had no organic brain disorders or neuro-psychiatric disease, and had not taken any neuro-psychiatric drugs.

Informed consents were obtained from all the subjects before participation in the PET study. This study protocol was approved by the Institutional Ethics Committee. All of the procedures conformed to the tenets of the Declaration of Helsinki.

All of the patients received an injection of botulinum-A toxin (18 to 36 units bilaterally) into the orbicularis oculi (OO) muscle, and the PET scans were obtained when the spasms of the OO were effectively restrained. PET scanning was done in the time when the spasm of eyelids was depressed after the botulinum toxin treatments within three months. The severity of blepharospasm was assessed with the 0 to 4 (0 = absent, 4 = most severe), and the frequency of blepharospasm was assessed with the 0 to 4 (0 = none, 4 = persistent eye closure), too in accordance with the classification of Jankovic [8]. We evaluated the severity and frequency of the

spasm in all the patients before the latest treatment of botulinum toxin and at the time of the PET study, actually between the injection of FDG and the scanning (Table 1). As not all the patients have reached complete suppression of blepharospasm at the moment of PET scan by botulinum-A toxin treatment, we divided the patients into two subgroups for further analysis, based on the on-site evaluation of the blepharospasm symptom: complete suppression group (n = 12; 5 men and 7 women; age 56.2 ± 9.5 years, severity 0, frequency 0) and incomplete suppression group (n = 13, 3 men and 10 women; age 48.8 ± 8.4 years, severity 1 ± 1, frequency 1 ± 1). There was no significant difference in symptomatic scores before treatment between incomplete suppression group (3.00, 3.00), and complete suppression group (3.08, 2.83). The only significant difference (p < 0.05) was the duration of illness: 1.50 ± 1.2 years in complete suppression group and 4.15 ± 4.1 years in incomplete suppression group.

MRI scans were obtained from all of the subjects to screen for organic brain disorders with a 1.5 Tesla scanner Signa Horizon (General Electric, Milwaukee). Transaxial images with T1-weighted contrast (3DSPGR, TR = 9.2 ms, TE = 2.0 ms, matrix size = 256 × 256 × 124, voxel size = 0.94 × 0.94 × 1.3 mm), and T2-weighted contrast (First Spin Echo, TR = 3,000 ms, TE = 100 ms, matrix size = 256 × 256 × 20, voxel size = 0.7 × 0.7 × 6.5 mm) were obtained. None of the subjects showed any abnormalities in brain morphology and intensities.

PET data acquisition

PET scans were obtained with the Headtome-V scanner SET 2400W (Shimadzu, Kyoto, Japan) at the Positron Medical Center, Tokyo Metropolitan Institute of Gerontology. Attenuation was corrected by a transmission scan with a $^{68}Ga/^{68}Ge$ rotating source. For the PET scan, a bolus of 120 MBq FDG was injected intravenously. Each patient was then requested to lie down comfortably with their eyes closed. A 6-minute emission scan in 3D acquisition mode was started 45 minutes after the injection, and 50 transaxial images with an interslice interval of 3.125 mm were obtained. The tomographic images were reconstructed using a filtered backprojection method, and Butterworth filter (cutoff frequency 1.25 cycle/cm and order of 2).

Data processing and statistical analysis

PET images were processed and analyzed with the statistical parametric mapping (SPM99) software [9] implemented in Matlab (Mathworks., Sherborn, MA, USA). Statistical parametric maps combine the general linear model and the theoretical Gaussian fields to make statistical inferences about regional effects. All PET images were spatially normalized to a standard template produced by Montreal Neurological Institute using the housemade template of FDG-PET images and smoothed with Gaussian filter for 16 mm FWHM to increase the signal to noise ratio before statistical processing.

After the appropriate design matrix was specified, the subject and group effects were estimated according to the general linear model at each voxel. We selected (compare-populations: 1 scan/subjects (two sample t-test)) in design type, and selected (global normalsation proportional scaling) in global normalization [10]. Statistical inference on the SPM (Z) was corrected using the theory of Gaussian Fields. To test hypotheses about regionally specific group effects, the estimates were compared using linear contrast. The threshold for SPM (Z) was set at p < 0.05 with a correction (p < 0.05, corrected) for the comparison between whole patient group and normal control group. We compared each of incomplete suppression group and complete suppression group to the normal control group in order to examine the effect of residual spasm. We also directly compared two subgroups each other. The threshold for SPM (Z) for the subgroup comparison was set at (p < 0.0001, uncorrected).

Table 1 Strength of the spasm of eyelids in EB patients

Age								
62	F	4 years	3 months	R (3, 3)	L (3, 3)	R (1, 1)	L (1, 1)
72	F	1 year	3 months	R (3, 3)	L (3, 3)	R (1, 1)	L (1, 1)
69	M	2 years	3 months	R (3, 3)	L (3, 3)	R (1, 1)	L (1, 1)
45	M	1 year	3 months	R (3, 3)	L (3, 3)	R (1, 1)	L (1, 1)
36	F	1 year	3 months	R (3, 3)	L (3, 3)	R (1, 1)	L (1, 1)
50	F	1 year	3 months	R (3, 3)	L (3, 3)	R (1, 1)	L (1, 1)
60	F	10 years	1 month	R (3, 3)	L (3, 3)	R (1, 1)	L (1, 1)
58	F	10 years	1 month	R (3, 3)	L (3, 3)	R (1, 1)	L (1, 1)
58	F	5 years	2 months	R (3, 3)	L (3, 3)	R (0, 0)	L (0, 0)
57	F	1 year	3 months	R (3, 3)	L (3, 3)	R (1, 1)	L (1, 1)
50	F	2 years	3 months	R (4, 3)	L (4, 3)	R (0, 0)	L (0, 0)
46	M	1 year	3 months	R (4, 3)	L (4, 3)	R (0, 0)	L (0, 0)
40	M	1 year	3 months	R (3, 3)	L (3, 3)	R (0, 0)	L (0, 0)
58	F	2 years	3 months	R (3, 3)	L (3, 3)	R (1, 1)	L (1, 1)
59	F	10 years	3 months	R (3, 3)	L (3, 3)	R (1, 1)	L (1, 1)
54	F	1 year	3 months	R (4, 3)	L (4, 3)	R (0, 0)	L (0, 0)
53	M	1 year	1 month	R (3, 3)	L (3, 3)	R (0, 0)	L (0, 0)
45	F	1 year	1 month	R (3, 3)	L (3, 3)	R (0, 0)	L (0, 0)
56	F	1 year	3 months	R (2, 2)	L (2, 2)	R (0, 0)	L (0, 0)
57	F	1 year	3 months	R (3, 3)	L (3, 3)	R (0, 0)	L (0, 0)
50	F	10 years	3 months	R (3, 3)	L (3, 3)	R (1, 1)	L (1, 1)
38	M	2 years	3 months	R (3, 3)	L (3, 3)	R (0, 0)	L (0, 0)
33	F	10 months	3 months	R (2, 2)	L (2, 2)	R (0, 0)	L (0, 0)
55	M	1 year	3 months	R (3, 3)	L (3, 3)	R (1, 1)	L (1, 1)
56	M	1 year	3 months	R (3, 3)	L (3, 3)	R (0, 0)	L (0, 0)

Average
Incomp group 4.2 ± 4.1 years   R (3.00, 3.00)   L (3.00, 3.00)
Comp group 1.5 ± 1.2 years   R (3.08, 2.83)   L (3.08, 2.83)
Total 2.9 ± 3.3 years   R (3.04, 2.92) L (3.04, 2.92) R (0.52, 0.52) L (0.52, 0.52)

Severity of spasm was rated on 0 (=none) to 4 (=severe) scale[8]
Frequency of spasm was rated on 0 (=none) to 4 (=functionally blind) scale[8]
Incomp Group: incomplete suppression group
Comp Group: complete suppression group

Results

A regional glucose hypermetabolism was found in the thalamus and pons bilaterally in patients with EB (p < 0.05, corrected), whose eyelid spasms were decreased by botulinum-A toxin (Table 2, Fig. 1). We made mean PET images of all patients and all normal subjects. Regions of interest (ROIs), 1 cm diameter circles, were placed the thalamus and pons, respec-

tively, due to measure the glucose metabolism levels of these regions. The mean increases were 6.5% in the thalamus and 5.3% in the pons. A trend of glucose hypermetabolism was also found in the putamen bilaterally in EB patients, but the increase was not significant (p < 0.01, uncorrected). There was no regional glucose hypometabolism above the statistical significant level. We found that significant hypermetabolism in the thalamus, pons and cerebellum bilaterally in incomplete suppression group

Table 2 Areas and coordinates for the maxima of regional glucose hypermetabolism in essential blepharospasm patients

				Z score
Thalamus (R)	12	−20	−2	5.00
Thalamus (L)	−8	−22	−2	5.54
Pons (R)	6	−40	−34	4.47
Pons (L)	−12	−40	−34	4.83

Areas with Z ≥ 4.17 (p < 0.05, corrected) were listed

Fig. 1 Areas of glucose hypermetabolism in patients with essential blepharospasm are showed (p < 0.05, corrected). Left; Sagittal and transverse views of a statistical parametric map (SPM) rendered into standard stereotactic space and projected onto a glass brain. Right; Six axial slices of brain are shown. The left side of the figure corresponds to the left hemisphere
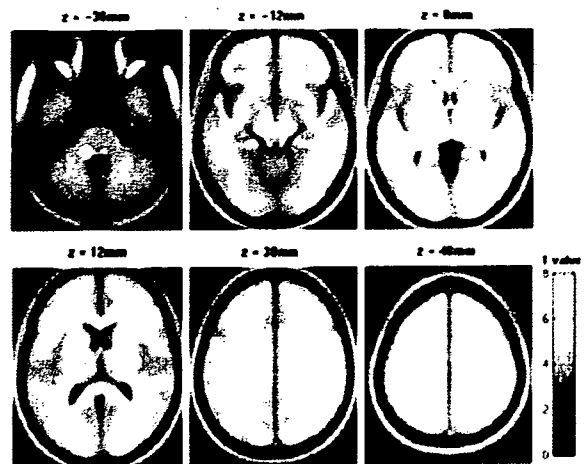
(p < 0.0001, uncorrected) (Table 3A, Fig. 2). On the other hand, hypermetabolism was observed only in the bilateral thalamus in complete suppression group (p < 0.0001, uncorrected) (Table 3B, Fig. 2). However, we could not find any significant difference between incomplete suppression group and complete suppression group by direct comparison (p < 0.001, uncorrected).

Discussion

Effect of involuntary movements

A majority of the studies on EB and other dystonias have demonstrated hypermetabolism of the thalamus and basal ganglia, however, there is a problem in interpreting these results because these studies were performed while the patients had active symptoms of dystonia, e.g., involuntary eyelid movements in EB patients. Thus, the observed abnormal cerebral activities could be due not only to the primary cause

of the dystonia, but also to the sensory input secondary from the involuntary movements. To overcome this criticism in EB patients, it is necessary to suppress the spasms of the eyelids. Hutchinson et al. hypothesized that there is metabolic increase in the thalamus and basal ganglia in EB patients because of an overactivity of a cortico-striato-thalamo-cortical motor circuit, and measured the glucose metabolism of 6 EB patients by PET while they were awake with active symptoms and while they were asleep without symptoms [4]. They found hypermetabolism in the cerebellum and pons during wakefulness, but not in the thalamus and basal ganglia during either condition. We suggest two possible reasons why they miss the hyperactivity in the thalamus and basal ganglia. First, the number of the patients and normal subjects in their study might not be enough. The difference of mean between two groups was relatively small compared to the standard deviation (difference of mean = 3.5, SD = 4.8 in the thalamus, for example), we have to increase the number of subject more than 20 to get a consistent statistical significance. Second,

Table 3 Areas and coordinates for the maxima of regional glucose hypermetabolism in incomplete suppression EB patients

Area				Z score
A				
Thalamus (R)	12	−10	2	3.52
Thalamus (L)	−6	−22	2	3.70
Pons (R)	2	−40	−32	5.06
Pons (L)	−6	−44	−32	5.16
Cerebellum (R)	40	−38	−38	3.58
Cerebellum (L)	−50	−48	−46	3.84
B				
Thalamus (R)	14	−20	−2	3.93
Thalamus (L)	−10	−20	−2	4.20

Areas with Z ≥ 3.45 (p < 0.0001, uncorrected) were listed

Fig. 2 Areas of glucose hypermetabolism in EB patients with incomplete suppression (left) and complete suppression (right) by botulinum toxin treatment are showed (p < 0.0001, uncorrected)
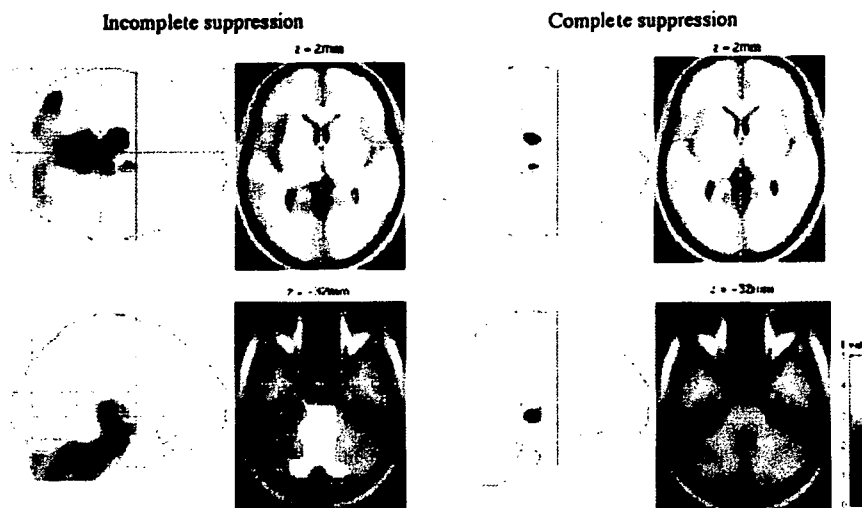
sleep might have depressed not only the involuntary movements but also the primary functional alteration in the brain of EB.

Ceballos-Baumann et al. examined patients with writer's cramp by PET during writing words before and after botulinum toxin treatment [11]. They found higher cerebral blood flow of patients before and after botulinum-toxin in the thalamus, left insula, bilateral premotor cortex, and bilateral primary sensory cortex than in normal subjects. In patients, activation in the cerebeller vermis was found before botulinum-toxin, but the activation disappeared after the treatment. We suggest that they succeeded in reducing the effect of involuntary movement, although the voluntary movements may still be a confounding factor.

Because the botulinum-toxin inhibits neuro-muscular conduction by a presynaptic blockade, we expected that the botulinum-toxin has minimum influence on the central causative mechanism of EB. Several previous studies have reported no significant alterations in the level of cerebral blood flow after botulinum toxin treatment [11, 12]. Therefore, in the present study, we performed a PET study in a larger size of the patients while awake and their spasms were effectively suppressed by the injection of botulinum toxin into the OO muscle bilaterally: 25 EB subjects and 38 normal controls. Under these conditions, we found a significant glucose hypermetabolism in the thalamus bilaterally in EB patients ($P < 0.05$, corrected).

Incomplete suppression group and complete suppression group

We divided EB patients to incomplete suppression group (13 patients) and complete suppression group (12 patients) based on the scores of blepharospasm at

the PET scanning. There was no significant difference in severity and frequency of spasm before treatment between these 2 groups. However, the mean duration of illness of incomplete suppression group was significantly longer than that of complete suppression group. Incomplete suppression group contained 4 patients whose duration of illness was over 10 years. These patients have repeatedly been treated by botulinum toxin for a long periods. The efficacy of the treatment might have been weakened due to tolerance [13].

Regional glucose metabolism in patients with EB

Hypermetabolism in the thalamus, basal ganglia, anterior cingulate gyrus and cerebellum of patients with spasmodic torticollis using PET were reported [5]. The results of functional imaging studies are often interpreted using the present anatomical model of information flow in cortico-striato-thalamo-cortical motor circuit (Fig. 3) [14]. Based on this model, there are three possible points which might alter thalamic activity. All of them are the alterations in inhibitory synaptic functions mediated by GABAergic system. Recent reports suggest that altered GABAergic inhibition may play a role in the symptomatology of dystonia. Previous studies found a reduction of GABA levels in the sensorimotor cortex and striatum of patients with focal dystonia [16]. We suspect that a reduction of GABA levels in the striatum or thalamus might cause the hyperactivity in these areas.

Macia et al. reported that injection of bicuculline, an antagonist to $GABA_A$, into the monkey thalamus induced dystonic symptoms contralaterally and found an overactivity of thalamic neurons ipsilateral to the treatment [17]. On the other hand, Kaji reported that one of the important functions of basal ganglia is the
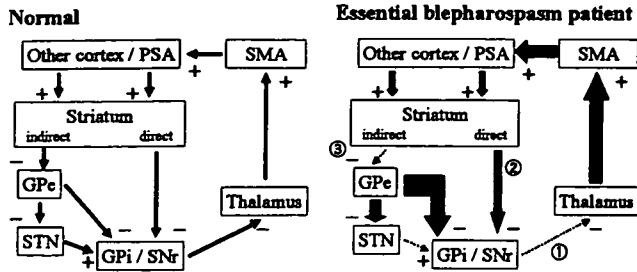
Normal　　　　　　　　**Essential blepharospasm patient**

Fig. 3 Principal pathways of the normal corticobasal ganglia–cortical loops and hypothetical alterations. In the normal loops (left), the striatum receives input from the primary somatosensory area (PSA) and from other areas of the motor and sensory cortex. The striatum projects by direct and indirect pathways to the major output structures of the basal ganglia, the globus pallidus interna (GPi) and substantia nigra reticulate (SNr). An indirect pathway includes a striatal–globus pallidus externa (GPe) projection. Some GPe fibers project to the subthalamic nucleus (STN) and GPi/SNr, and other fibers project directly to the GPi/SNr. GPi/SNr, which in turn, projects to the thalamus with a subsequent feedback to motor cortex, primarily the SMA. The effect of each structure on subsequent structures is to increase (+) or decrease (−) neuronal activity as indicated, adapted from Tempel et al. [14] and Garfen [15]. For glucose hypermetabolism in the thalamus and striatum of EB patients (right), the possible points of impairments with the circuit are; 1) to impaired inhibition from GPi/SNr, 2) decreased GPi/SNr activity may result in increased activity of the direct pathway from Striatum to GPi/SNr, and 3) impaired the indirect pathway at the level of Striatum-GPe connection

gating of sensory input for motor control [18], and its alteration might cause dystonia. Previous reports found glucose hypermetabolism in EB and other focal dystonias in the striatum as well as in the thalamus [3, 5]. Recently, Schmidt et al. reported that a subregion of the putamen was active during EB spasms in patients but not during voluntary blinks in normal subjects using fMRI [19]. Perlmutter et al. have demonstrated that individuals with EB and hand dystonia have a reduced level of dopamine D_2-like receptors in the putamen relative to control subjects [20], suggesting that dopamine D_2-receptor loss disrupts lateral inhibition created by the indirect pathway of the basal ganglia. These evidences have suggested that the altered function of the putamen may be a critical component of EB. We found a trend of glucose hypermetabolism in the putamen bilaterally in EB patients, but the increase was not significant ($p < 0.01$, uncorrected). It is plausible that the hyperactivity of the striatum is sensory-input dependent. On the other hand, the hyperactivity in the thalamus was more consistent even with the depletion of sensory feedback. From these observations, hyperactivation of the thalamus may be one of the primary causes of EB, however, it might reflect a compensatory mechanism. Further investigation is required to clarify the different role of the thalamus and the striatum in the pathophysiological mechanism of EB.

We found significant hypermetabolism in the cerebellum and pons in incomplete suppression group

($p < 0.0001$, uncorrected), and not in complete suppression group ($p < 0.0001$, uncorrected) when the images of these groups were contrasted to the control group. We did not find significant difference by direct comparison of subgroups, presumably because the number of the patients in these subgroups might not be enough to reach statistical significance. The cerebellum receives extensive somatosensory input via spinocerebellar pathways, and the cerebellum would be a sensory organ [21]. Hutchinson et al. reported that EB patients exhibit hypermetabolism of the cerebellum and pons during wakefulness, but not during sleeping using PET [4]. And, Ceballos-Baumann et al. reported that patients with writer's cramp activation in the cerebeller vermis was found before botulinum-toxin, but the activation disappeared after the treatment [11]. Our results indicate that activation of the cerebellum in EB patients could be due to increased sensory input derived from involuntary muscle contraction of eyelids. Aramideh et al. reported a secondary blepharospasm patient with a small dorsomedial pontine lesion [22], and LeDoux et al. reported a secondary cervical dystonia patients due to infarctions or hemorrhage in the pons [23]. They hypothesized that abnormalities of olivocerebellar circuit and cortico-striato-thalamo-cortical motor circuit might produce similar movement disorders, and they suggested that lesions in the pons obstructed the cerebellar afferent pathways, and produced cervical dystonia.

We found significant hypermetabolism of the tegmentum in the inferior pons, and this area corresponds to the facial nucleus and facial nerve. The facial nerve is the final output pathway of focal facial dystonia from the nervous system. As the effect of botulinum-A toxin is peripheral, the facial nuclei and related structure in pons may remain hyperactive even after the treatment as we observe in our results. From these things, we suspected that hypermetabolism in the cerebellum and pons was the secondary phenomenon related to muscular activity of eyelids.

Conclusions

A glucose hypermetabolism was detected in the thalamus and pons bilaterally in EB patients. Hyperactivity in the thalamus may be related to the primary cause of compensatory mechanism of EB sharing the common pathophysiological mechanism to other types of focal dystonia.

References

1. Berardelli A, Rothwell JC, Hallett M, Thompson PD, Manfredi M, Marsden CD (1998) The pathophysiology of primary dystonia. Brain 121:1195–1212
2. Kostic VS, Stojanovic-Svetel M, Kacar A (1996) Symptomatic dystonias associated with structural brain lesions: report of 16 cases. Can J Neurol Sci 23:53–56
3. Esmaeli GB, Nahmias C, Thompson M, et al. (1999) Positron emission tomography in patients with benign essential blepharospasm. Ophthal Plast and Reconstr Surg 15:23–27
4. Hutchinson M, Nakamura T, Moeller JR, et al. (2000) The metabolic topography of essential blepharospasm. A focal dystonia with general implications. Neurology 55:673–677
5. Galardi G, Perani D, Grassi F, et al. (1996) Basal ganglia and thalamo-cortical hypermetabolism in patients with spasmodic torticollis. Acta Neurol Scand 94:172–176
6. Eidelberg D, Moeller JR, Ishikawa T, et al. (1995) The metabolic topography of idiopathic torsion dystonia. Brain 118:1473–1484
7. Wakakura M, Tsubouchi T, Inouye J (2004) Etizolam and benzodiazepine induced blepharospasm. J Neurol Neurosurg Psychiatry 75:506–509
8. Jankovic J, Orman J (1987) Botulinum A toxin for cranial-cervical dystonia: A double-blind, placebo-controlled study. Neurology 37:616–623

9. Friston KJ, Frith CD, Liddle PF, Frackowiak RS (1991) Comparing functional (PET) images: the assessment of significant change. J Cereb Blood Flow Metab 11:690–699
10. Friston KJ, Frith CD, Liddle PF, Dolan RJ, Lammertsma AA, Frackowiak RSJ (1990) The relationship between global and local changes in PET scans. J Cereb Blood Flow Metab 10:458–466
11. Ceballos-Baumann AO, Sheean G, Passingham RE, et al. (1997) Botulinum toxin does not reverse the cortical dysfunction associated with writer's cramp. A PET study. Brain 120:571–580
12. Ridding MC, Sheean G, Rothwell JC (1995) Changes in the balance between motor cortical excitation and inhibition in focal, task specific dystonia. J Neurol Neurosurg Psychiatry 59:493–498
13. Hsiung GY, Das SK, Ranawaya R, Lafontaine AL, Suchowersky O (2002) Long-term efficacy of botulinum toxin A in treatment of various movement disorders over a 10-year period. Mov Disord 17:1288–1293
14. Tempel LW, Perlmutter JS (1993) Abnormal cortical responses in patients with writer's cramp. Neurology 43:2252–2257
15. Garfen CR (1992) The neostriatal mosaic: multiple levels of compartmental organization. Trends Neurosci 15:133–139

16. Levy LM, Hallett M (2002) Impaired brain GABA in focal dystonia. Ann Neurol 51:93–101
17. Macia F, Escola L, Guehl D, Michelet T, Bioulac B, Burbaud P (2002) Neuronal activity in the monkey motor thalamus during bicuculline-induced dystonia. Eur J Neurosci 15:1353–1362
18. Kaji R (2001) Basal ganglia as a sensory gating devise for motor control. J Med Invest 48:142–146
19. Schmidt KE, Linden DEJ, Goebel R, Zanella FE, Lanfermann H, Zubcov AA (2003) Striatal activation during blepharospasm revealed by fMRI. Neurology 60:1738–1743
20. Perlmutter JS, Stambuk MK, Markham J, et al. (1997) Decreased [18F] spiperone binding in putamen in idiopathic focal dystonia. J Neurosci 17:843–850
21. Gao JH, Parson LM, Bower JM, Xiong J, Li J, Fox PT (1996) Cerebellum implicated in sensory acquisition and discrimination rather than motor control. Science 272:545–547
22. Aramideh M, Ongerboer de Visser BW, Holstege G, Majoie CBLM, Speelman JD (1996) Blepharospasm in association with a lower pontine lesion. Neurology 46:476–478
23. LeDoux MS, Brady KA (2003) Secondary cervical dystonia associated with structural lesions of the central nervous system. Mov Disord 18:60–69

Correlation between each task of the Mini-Mental State Examination and regional glucose hypometabolism in at-rest Alzheimer's disease patients

Masahiro Mishina,[1,2,3] Kenji Ishii,[2] Shin Kitamura,[3,4] Masahiko Suzuki,[2,5] Shiro Kobayashi,[1] Kiichi Ishiwata[2] and Yasuo Katayama[3]

[1]Neurological Institute, Nippon Medical School Chiba-Hokusoh Hospital, Chiba, [2]Positron Medical Center, Tokyo Metropolitan Institute of Gerontology, Tokyo, [3]The Second Department of Internal Medicine, Nippon Medical School, [4]Department of Internal Medicine, Nippon Medical School Second Hospital, Chiba, and [5]Department of Neurology, The Jikei University School of Medicine, Tokyo, Japan

We investigated the relationship between each task of the Mini-Mental State Examination (MMSE) and regional glucose hypometabolism in patients with Alzheimer's disease (AD). We studied 38 patients with probable AD using 2-^{18}F-fluoro-2-deoxy-D-glucose positron emission tomography (FDG PET). The images were corrected for differences in FDG uptake by cerebellar normalization, and were spatially normalized into a standard stereotactic anatomical space using statistical parametric mapping (SPM). There was a positive correlation between FDG uptake and the MMSE subscores for temporal orientation in the bilateral temporal and frontal cortex, and cingulate gyrus; for spatial orientation in the left parietal cortex, bilateral frontal and temporal cortex, and cingulate gyrus; for attention and calculation in the left temporal and frontal cortex; for writing in the left temporal cortex; and for copying and drawing, the correlation was positive in the bilateral parietal and occipital cortex. The total MMSE score was positively correlated with FDG uptake in the left temporal and frontal lobe. Our study demonstrated that, in AD patients, the distribution of hypometabolism in the resting state was related to clinical symptoms and that MMSE scores reflected brain dysfunction in the left hemisphere. Correlation analysis using SPM and FDG PET is useful for the objective evaluation of cognitive tests and diagnostic scoring.

Keywords: Alzheimer's disease, glucose metabolism, Mini-Mental State Examination, positron emission tomography, statistical parametric mapping.

Introduction

The cerebral glucose metabolism is thought to reflect regional neuronal activities.[1-3] Positron emission tomography (PET) with 2-^{18}F-fluoro-2-deoxy-D-

glucose (FDG), and statistical image analysis applications such as statistical parametric mapping (SPM) and three-dimensional (3D) stereotactic surface projections,[4,5] have shown that the cerebral glucose metabolism in patients with Alzheimer's disease (AD) is reduced in the temporal, parietal, posterior cingulate and prefrontal regions. However, these findings did not correspond with the distribution of neuronal loss on postmortem studies.[6] In an ^{11}C-flumazenil PET study in AD, Ohyama *et al.*[7] showed that neuronal density was less impaired than neuronal function assessed by the

cerebral blood flow and glucose metabolism in the associated cortex. This discrepancy may be attributable to the observation that most of the cerebral glucose metabolism reflects the synaptic activities projecting from neurons.[1,8] Based on this hypothesis, FDG PET can be used for brain-function mapping.[9-11] Recent image analysis applications, such as SPM, allow us to analyze all available metabolic information, without a priori hypotheses based on anatomic knowledge which is essential for regions of interest (ROI) analysis.[12,13] In patients with brain damage, it is possible to calculate the region at which there is a correlation between the functional disturbance and glucose hypometabolism.[14]

The Mini-Mental State Examination (MMSE) is the most commonly used method to evaluate cognitive function and to screen for dementia.[15] Some studies reported the regional glucose hypometabolism of AD correlated with total score of MMSE,[4,16] and neuropsychological subjects.[17-21] However, no data are available on the relationship between each task in the MMSE and the regional brain dysfunction of AD. Taking into consideration each MMSE parameter, we used MMSE subscores and FDG PET to investigate the relationship between the cognitive tasks of MMSE and regional glucose hypometabolism in AD patients.

Materials and methods

Subjects

We retrospectively evaluated 117 consecutive AD patients who underwent FDG PET at the Positron Medical Center of Tokyo Metropolitan Institute of Gerontology between January 2001 and December 2004. Their diagnosis was based on criteria promulgated by the National Institute of Neurological and Communicative Diseases and the Stroke/Alzheimer's Disease and Related Disorders Association (NINCDS-ADRDA).[22] Inclusion criteria were the availability of MMSE total and subscores. Based on the results of the MMSE, performed within 1 week of PET scanning, we selected 38 patients with probable AD for this study. They were 18 men and 20 women ranging in age 59–86 years (mean, 73.3 ± 6.3). Mean of the duration of AD was 4.2 ± 3.5 years (0.7–17). Values of the age and duration were used as the nuisance variable of ANCOVA.[6,23,24] Normal subjects were not included as controls in this study.

The study protocol was approved by the Ethics Committee of the Tokyo Metropolitan Institute of Gerontology; prior written informed consent was obtained from all study participants.

Positron emission tomography imaging

Positron emission tomography was performed with an SET-2400 W scanner (Shimadzu, Kyoto, Japan) at the

Positron Medical Center of Tokyo Metropolitan Institute of Gerontology;[25] all subjects had fasted for more than 5 h prior to scanning. Transmission data were acquired with a rotating ^{68}Ga/^{68}Ge rod source for attenuation correction. The FDG uptake was acquired with static scans after the injection of 120 MBq of FDG. During the tracer-accumulation phase, the patients remained supine, quiet and motionless in a dimly lit room; their eyes and ears were open. At 45 min post-injection, a 12-min emission scan was obtained in the 3D mode. The blood glucose concentration was measured before and after the scanning to confirm its stability during the course to the PET recordings.

Data analysis

Image manipulations were carried out on an O2 workstation (Silicon Graphics, Mountain View, CA, USA) and a PowerBook G4 (Apple Computer, Cupertino, CA, USA), using the medical image-processing application package Dr View version 5.3.1 (Asahi Kasei Joho System, Tokyo, Japan) and SPM2 (Wellcome Department of Cognitive Neurology, Institute of Neurology, London, UK) implemented in MATLAB version 5.6.1 (Mathworks, Natick, MA, USA). Using a locally produced FDG template and SPM2, the FDG images were spatially normalized into a standard stereotaxic anatomical space with a cubic (2 mm × 2 mm × 2 mm) voxel size.[12] Circular ROI 10 mm in diameter were drawn on the cerebellar hemisphere on each normalized PET image. Canonical magnetic resonance imaging (MRI) attached to SPM2 was also used to obtain information for placement of the ROI on normalized PET images. The ROI value was employed for proportional scaling. The data were corrected for individual differences in FDG uptake by proportional scaling using the cerebellar ROI value.[26] Then, the data were smoothed with a 16-mm Gaussian filter to account for residual inter-subject differences. Using SPM2 segmentation and a mean image of the MRI scan attached to SPM2, we generated a masking image of the cerebrum to remove voxels outside the cortex. With the masking image in place, we computed statistical parametric maps on a voxel-by-voxel basis using whole voxels within the brain surface to avoid missing low-metabolic brain regions. ANCOVA were also used to eliminate the effect of age and duration of the disease for each subject as the nuisance variable. The T-maps for correlations between the MMSE subscores and the FDG uptake were obtained using a multiple regression model and displayed with a voxel threshold probability of 0.001 and an extent threshold of 300 contiguous voxels per cluster (uncorrected for multiple comparisons). For the total MMSE score, we calculated the T-map for correlations with the FDG uptake at a voxel

| 125

Table 1 Mean subscore for each Mini-Mental State Examination (MMSE) parameter in 38 patients with Alzheimer's disease

No.	Subject	Mean ± SD
1	TEMPORAL ORIENTATION – 1 point for each answer	1.84 ± 1.48
	Q: "What is the: (year)(season)(date)(day)(month)?"	
2	SPATIAL ORIENTATION – 1 point for each answer	2.58 ± 1.45
	Q: "Where are we: (state)(county)(town)(hospital)(floor)?"	
3	REGISTRATION – 1,2 or 3 points according to how many are repeated	2.87 ± 0.34
	Name three objects: Give the patient 1 s to say each.	
	Ask the patient to: repeat all three after you have said them.	
	Repeat them until the patient learns all three.	
4	ATTENTION AND CALCULATION – 1 point for each correct subtraction	1.74 ± 1.61
	Ask the patient to: begin from 100 and count backwards by 7.	
	Stop after 5 answers (93, 86, 79, 72, 65).	
5	RECALL– 1 point for each correct answer	0.53 ± 0.98
	The patient is asked to name the 3 objects cited above.	
6	NAMING (2 points)	1.95 ± 0.32
	The patient is asked to identify and name a pencil and a watch.	
7	REPETITION (1 point)	0.79 ± 0.41
	Ask the patient to: repeat the phrase "No ifs, ands, or buts."	
8	VERBAL INSTRUCTION (1 point for each task completed properly)	2.79 ± 0.53
	The patient is asked to take a paper in the right hand, fold it in half, and put it on the floor.	
9	READING AND OBEYING (1 point)	0.89 ± 0.31
	The patient is asked to read and obey the command "Close your eyes."	
10	WRITING (1 point)	0.68 ± 0.47
	The patient is asked to write a sentence.	
11	COPYING AND DRAWING (1 point)	0.71 ± 0.46
	The patient is asked to copy a complex diagram of two interlocking pentagons.	

threshold *P*-value of 0.05 (corrected for multiple comparisons).

Results

The mean score of the MMSE was 17.4 ± 4.4 (mean ± SD) for the 38 patients. As shown in Table 1, the MMSE subscores for temporal orientation, attention and calculation, and recall were low in many patients. On the other hand, many patients scored well for registration, naming, repetition, verbal instruction, and reading and obeying.

Table 2 summarizes the results of SPM for the correlation between FDG uptake and MMSE subscores. There was a positive correlation between the FDG uptake and MMSE subscores for temporal orientation in the left middle temporal and inferior temporal gyrus, right inferior temporal, superior frontal, middle frontal, straight and cingulate gyrus (Fig. 1a), for spatial orientation in the left angular, middle occipital, middle temporal, inferior temporal, superior temporal, inferior frontal, superior frontal, medial frontal, middle frontal, straight, cingulate gyrus, and insular gyri, inferior parietal lobe, pre-cuneus, and cuneus, right pre-cuneus,

cuneus, cingulate, superior frontal, middle frontal and straight gyrus (Fig. 1b), for attention and calculation in the left superior temporal, middle temporal, inferior temporal, fusiform, parahippocampal, superior temporal, middle frontal, inferior frontal, cingulate, precentral and inferior frontal gyrus, and hippocampus (Fig. 1c), for writing in the left inferior temporal, middle temporal, superior temporal gyrus (Fig. 1d), and for copying and drawing in the right inferior parietal, superior parietal lobe, superior occipital, angular and middle occipital gyrus, pre-cuneus, and cuneus, left superior parietal, inferior parietal lobe, angular and superior occipital gyrus, cuneus, and pre-cuneus (Fig. 1e). There was no correlation between the FDG uptake and the MMSE subscores for registration, recall, naming, repetition, verbal instruction, and reading and obeying.

The total MMSE score was positively correlated with the FDG uptake in the left inferior temporal, middle temporal, superior temporal, fusiform-, parahippocampal, supramarginal, angular, inferior frontal, middle frontal straight, medial frontal, cingulate, superior frontal, pre-central gyrus, hippocampus, orbital and insular gyri, right straight, medial frontal and cingulate gyrus, and orbital gyri (Fig. 1f, Table 3).

126 |